LETTER

doi:10.1038/nature12176

Distinct behavioural and network correlates of two interneuron types in prefrontal cortex

D. Kvitsiani[1]*, S. Ranade[1]*, B. Hangya[1], H. Taniguchi[1]†, J. Z. Huang[1] & A. Kepecs[1]

Neurons in the prefrontal cortex exhibit diverse behavioural correlates[1–4], an observation that has been attributed to cell-type diversity. To link identified neuron types with network and behavioural functions, we recorded from the two largest genetically defined inhibitory interneuron classes, the perisomatically targeting parvalbumin (PV) and the dendritically targeting somatostatin (SOM) neurons[5–8] in anterior cingulate cortex of mice performing a reward foraging task. Here we show that PV and a subtype of SOM neurons form functionally homogeneous populations showing a double dissociation between both their inhibitory effects and behavioural correlates. Out of several events pertaining to behaviour, a subtype of SOM neurons selectively responded at reward approach, whereas PV neurons responded at reward leaving and encoded preceding stay duration. These behavioural correlates of PV and SOM neurons defined a behavioural epoch and a decision variable important for foraging (whether to stay or to leave), a crucial function attributed to the anterior cingulate cortex[9–11]. Furthermore, PV neurons could fire in millisecond synchrony, exerting fast and powerful inhibition on principal cell firing, whereas the inhibitory effect of SOM neurons on firing output was weak and more variable, consistent with the idea that they respectively control the outputs of, and inputs to, principal neurons[12–16]. These results suggest a connection between the circuit-level function of different interneuron types in regulating the flow of information and the behavioural functions served by the cortical circuits. Moreover, these observations bolster the hope that functional response diversity during behaviour can in part be explained by cell-type diversity.

To investigate whether distinct interneuron types can encode specific behavioural variables we recorded the activity of inhibitory neurons expressing parvalbumin and somatostatin markers (Supplementary Fig. 1a). PV basket cells are thought to control the spiking output of pyramidal neurons[12,14], whereas most SOM interneurons, known as Martinotti cells (Supplementary Fig. 1c, d), target distal dendrites, gating the inputs arriving onto pyramidal cells[13,15,17–20]. To target these interneuron types for recordings, we used PV-Cre and SOM-Cre[21,22] driver mouse lines in combination with adeno-associated viruses to deliver channelrhodopsin-2 (ChR2)[23], rendering neurons light sensitive (Supplementary Fig. 1a, b). Miniature microdrives housing 6 movable tetrodes and an optical fibre were implanted in deep layers of the anterior cingulate cortex (ACC) (Fig. 1a and Supplementary Fig. 1e–g). We recorded well-isolated single units ($n = 1{,}339$ from 6 PV-Cre and 6 SOM-Cre mice) and delivered brief pulses (1 ms) of blue light to elicit short-latency action potentials in ChR2-expressing neurons that served as a physiologic tag[24] (Fig. 1b, c). To identify directly light-activated units we developed an optical-tagging test based on a statistical measure that yields a P value testing whether light-activation induced significant changes in spike timing (Fig. 1d and Supplementary Fig. 2, see Methods). Significantly activated units ($P < 0.01$) showed similar spontaneous and light evoked waveforms (correlation coefficient, $r > 0.85$, Fig. 1b and Supplementary Fig. 2c), low-latency light-induced response (< 4 ms), and low first-spike jitter (Fig. 1e, f), signatures of direct light-activation.

Extracellularly recorded units are traditionally classified based on spike width and firing rate, with narrow-spiking and fast-firing neurons categorized putatively as PV interneurons[1,25]. Indeed, most identified PV neurons were narrow-spiking with high firing rates (219 ± 10 μs, 31 ± 3 Hz, $n = 23$, Fig. 1e), whereas the spike-width distribution for SOM units was bimodal (Fig. 1e, bottom): a third of neurons had narrow spikes ('NS', <270 μs) and high firing rates (212 ± 7 μs, 16 ± 4 Hz, $n = 13$) and the rest showed markedly wider spike waveforms and lower firing rates ('WS', 327 ± 7 μs, 4 ± 1 Hz, $n = 22$).

Having identified PV and SOM interneurons, we first examined their effect on local circuit activity. Synchronous photostimulation of ChR2-expressing PV or SOM neurons had markedly different network effects, with PV neurons imposing brief uniform inhibition on nearby neurons[26], and SOM neurons exerting longer and more variable inhibition (Fig. 2a, b and Supplementary Fig. 3a, b). These differences cannot be accounted for by systematic differences in the number of photo-activated neurons (Supplementary Fig. 4) and indicate that SOM and PV neurons exert distinct inhibitory footprints on network activity.

Optogenetic identification of many individual interneurons, in combination with simultaneous recording from a large number of their neighbours, allowed us to investigate the physiological impact of different inhibitory subtypes during behavioural epochs without light stimulation. To identify possible functional connectivity between neurons, we computed cross-correlograms (CCGs)—counts of spike co-occurrences in the putative pre- and postsynaptic neuron pairs at different time lags[27] (Fig. 2c). Significant short-latency interactions were rare among pairs of unidentified ACC neurons (3.2% inhibitory, 5.2% excitatory, 1.3% both, out of 2,945 pairs, bootstrap test with $P < 0.001$ used for all CCG significance testing). Remarkably, 5/7 pairs of PV neurons showed interactions with 3/7 firing in millisecond zero-lag synchrony, and 4/7 inhibited each other (trough at 2.25 ± 0.5 ms, Fig. 2c and Supplementary Fig. 5a, c). PV neurons also showed a high prevalence of short-timescale correlations with unidentified neurons (38/152 pairs, $P < 0.001$, Fig. 2c and Supplementary Fig. 5c), often with detectible inhibition (trough at 2.39 ± 1.3 ms, 18/152 pairs, $P < 0.001$). These results demonstrate that the PV population is capable of millisecond synchronization with fast and precise inhibitory effect on local neural activity.

In contrast to PV pairs, we found no short-timescale correlations between SOM pairs (0/11, 7 WS–WS and 4 NS–WS pairs, Fig. 2c and Supplementary Fig. 5b), and the influence of both NS-SOM and WS-SOM on unidentified neurons was sparser and more diverse (15/169 pairs, inhibitory in 2/169, $P < 0.001$, Fig. 2c and Supplementary Fig. 5c). The weak observable effect of SOM neurons on the firing output of their neighbours could be due to dendritic inhibition generating input suppression, which is expected to be more difficult to detect using a cross-correlation approach. Thus, PV and SOM interneurons

[1]Cold Spring Harbor Laboratory, 1 Bungtown Road, Cold Spring Harbor, New York 11724, USA. †Present address: Max Planck Florida Institute for Neuroscience, One Max Planck Way, Jupiter, Florida 33458-2906, USA.
*These authors contributed equally to this work.

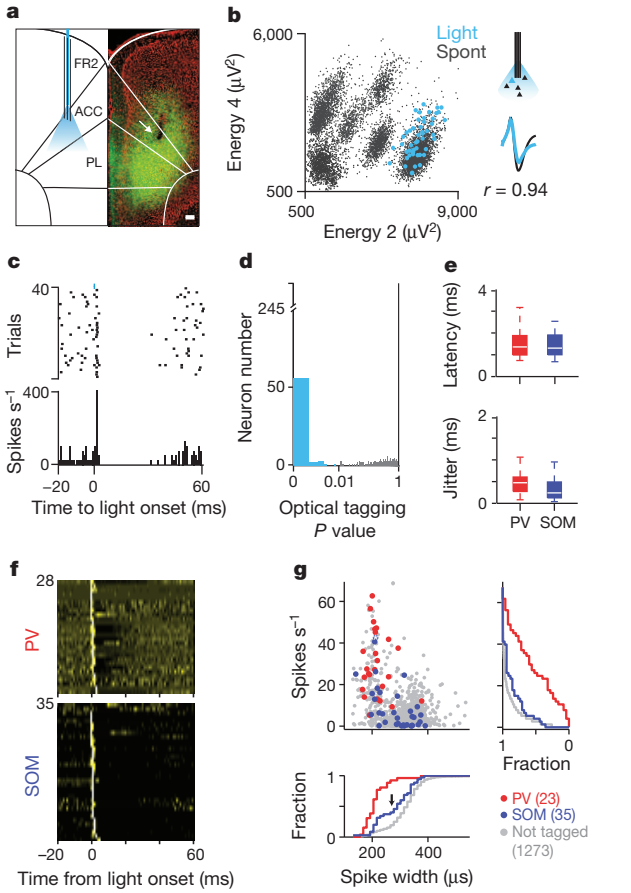

Figure 1 | Optogenetic tagging of genetically-defined interneurons in behaving mice. **a**, Coronal section from a SOM-IRES-Cre mouse (green, ChR2; red, DAPI (4′,6-diamidino-2-phenylindole)). Arrow indicates electrolytic lesion of recording site in the ACC. Scale bar, 100 μm. ACC, anterior cingulate; FR2, frontal region 2; PL, prelimbic cortex. **b**, Spike sorting example. Unclustered spikes plotted in waveform energy space from two tetrode channels (energy 2, energy 4). Light-evoked spikes superimposed in blue. Bottom right, average spontaneous and light-evoked waveforms. **c**, Spike raster (top) and peri-stimulus time histogram (PSTH) (bottom) for the light-activated cell in **b**, aligned to light onset. Light pulse shown in blue (duration, 1 ms; power, ~100 mw per mm^2; frequency, 10 Hz). **d**, Histogram of SALT (stimulus-associated spike latency test) for optical tagging yielded strongly bimodal distribution of *P* values; ($P < 0.01$, blue). **e**, Box plots for all tagged PV (red) and SOM (blue) neurons show low light-evoked first-spike latency (top) and small jitter (bottom). **f**, *z*-scored PSTH of all tagged PV (top) and SOM (bottom) interneurons in response to 1-ms blue light stimulation. **g**, Firing rate as a function of spike width for PV, SOM and not tagged neurons. White asterisk indicates neuron in **b** and **c**. Cumulative histograms of firing rate (top right) and spike width (bottom) are plotted for all groups. Arrow marks mode separation of spike width (NS and WS) distribution for SOM neurons.

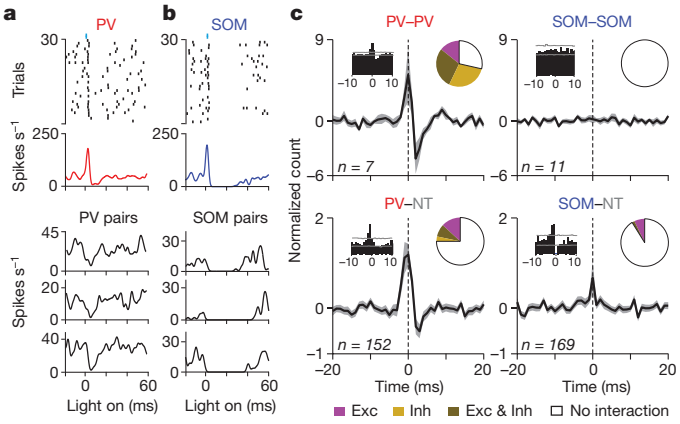

Figure 2 | Distinct inhibitory effect of SOM and PV interneurons. **a**, **b**, Top, spike raster and PSTH of PV (**a**) and SOM (**b**) interneurons aligned to light onset. Bottom, PSTH of three simultaneously recorded unidentified neurons (PV pairs and SOM pairs). **c**, Average cross-correlograms (CCG) between PV–PV (top left), PV–Not tagged (NT) (bottom left), SOM–SOM (top right), and SOM-Not tagged (NT) (bottom right) neuron pairs (shaded area indicates s.e.m.); examples of significant pairwise interactions (left inset) and summary for statistically significant CCG interactions (right inset). Exc, excitatory; Inh, inhibitory.

form distinct inhibitory networks: a fast, synchronous PV network generating strong, transient inhibition and an asynchronous SOM network with weaker effect on firing output.

We explored whether these cell-type differences in network functions are also reflected in specific behavioural correlates. To engage neural ensembles in the ACC we used a task that incorporated cue-based prediction, temporal control of actions and reward foraging decisions (Fig. 3a). Mice were trained to run back and forth on a linear track between two platforms to collect water rewards; entering one platform ('trigger zone') enabled reward availability at the other ('reward zone'). As mice ran back to the reward zone platform, reward size was cued by an auditory signal. This task mimics the self-paced timing of foraging behaviours and exploits the natural tendency of mice to trade staying in a rewarded, safe area with running on an elevated open track to enable future reward collection. Behavioural performance was sensitive to anticipated reward outcomes because on a subset (15%) of trials in which the cue and reward were omitted, mice slowed their speed during reward zone approach (Fig. 3b).

We examined the responses of a population of 1,034 neurons (from 4 PV-Cre and 6 SOM-Cre mice) in the task. Neurons responded at several behavioural events and modulated their firing by different behavioural variables. For instance, as expected of neurons in the ACC[3,9,11], we found single neuron correlates of reward prediction, staying time, and reward outcome and size (Supplementary Fig. 6a). The firing of many individual neurons was selective for single as well as combinations of task variables without any apparent clustering of response properties (Supplementary Fig. 6b–e). Therefore, we used an unbiased approach to determine firing rate modulation patterns for the PV and SOM neurons, which focused our analysis on two behaviourally relevant events, reward approach and leaving (see Methods and Supplementary Fig. 6f). Similar to the example neuron (Fig. 3c), most recorded PV neurons (11/14) phasically increased their firing as mice left the reward zone (Fig. 3d and Supplementary Figs 7c and 8a, b). To test the homogeneity and specificity of these event-related response profiles we used a resampling approach and compared PV interneurons to the unidentified population (see Methods). We found that the temporal response profiles of the PV interneurons were homogeneous ($P < 0.01$, bootstrap test) and distinct ($P < 0.001$) compared to randomly selected groups of neurons (see also Supplementary Fig. 9d). Moreover, knowledge of PV identity carried approximately twice the information about the time course of responses than knowledge that a neuron is narrow-spiking, despite the fact that PV neurons tend to be narrow-spiking ($P < 0.05$, Supplementary Fig. 7b).

The firing of many SOM neurons was strongly suppressed at the time of reward zone entry (13/21, suppression index < 0, $P < 0.01$, permutation test), like the example neuron (Fig. 3e). Similarly, most NS-SOM neurons were suppressed upon entry into the reward zone (9/10, Fig. 3f, bottom, and Supplementary Fig. 8a, b). In contrast, WS-SOM neurons were activated at different moments in time, around the entry into the reward zone (Fig. 3f, top). These profiles were different from both the PV and the unidentified population (Supplementary Fig. 7a, d). Together with their local-circuit effects described above, these observations support the idea that SOM neurons comprise at least two functional subtypes[18,19,28], a narrow-spiking, more

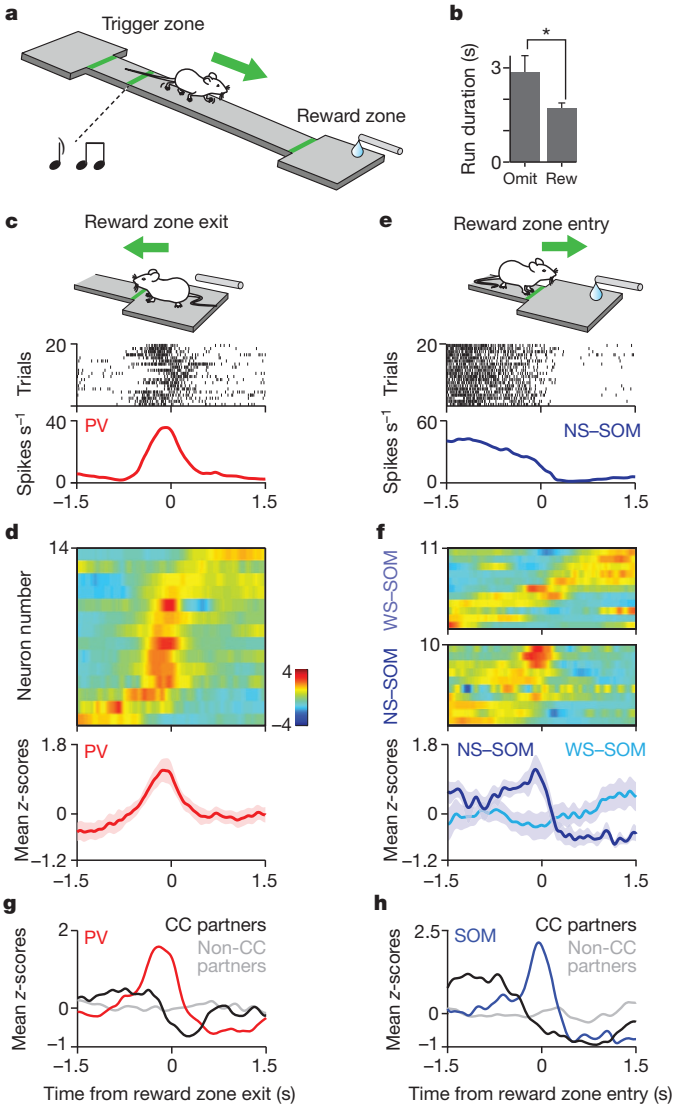

Figure 3 | Distinct behavioural correlates of PV and SOM interneurons. **a**, Cartoon of mouse performing the reward foraging task. **b**, Average run duration for rewarded (Rew) and omission (Omit) trials ($n = 63$ sessions, $P < 0.05$, Mann–Whitney U-test). **c**, Spike raster and peri-event time histogram (PETH) for an identified PV interneuron aligned to time of reward zone exit. **d**, Top, z-scored PETHs of 14 PV neurons sorted by latency to half-peak firing (colors from blue to red indicate low to high normalized firing rate of neurons, respectively); bottom, mean z-scored response (shaded area indicates s.e.m.). **e**, Spike raster and PETH for a NS-SOM interneuron aligned to the time of reward zone entry. **f**, Top, z-scored PETHs of 21 SOM neurons. NS-SOM and WS-SOM neurons are separated. Bottom, mean responses for NS-SOM and WS-SOM neurons (shaded area indicates s.e.m.). **g**, Average PETH for PV interneurons (red, $n = 4$) with significant inhibitory cross-correlations, (CC-partners, black, $n = 5$) and non-CC partners (grey, $n = 76$). **h**, Average PETH for SOM interneurons (blue, $n = 3$), CC-partners (black, $n = 3$) and non-CC partners (grey, $n = 34$).

homogeneously responding population and a wide-spiking population with heterogeneous response profiles.

We examined whether these cell-type-specific differences in behavioural correlates are also reflected in their synaptic partners. We characterized the responses of unidentified wide-spiking (putative pyramidal, pPyr) neurons that showed significant inhibitory cross-correlations with identified interneurons (CC-partners, for example, Fig. 2c, lower panels, inset). Notably, PV→pPyr and SOM→pPyr pairs, which both showed negative cross-correlations on the time scale of milliseconds, exhibited opposing behavioural response-dynamics on the time scale of seconds (Fig. 3g, h). This was not observed for simultaneously recorded neurons without significant short-term interactions with PV or SOM neurons (Fig. 3g, h). These results reveal that functional connectivity, as identified by millisecond cross-correlations indicative of anatomical connections, also predicts post-synaptic neural responses on the time scale of seconds as relevant for behaviour.

Finally, we sought to better understand the behavioural functions of the PV population. We wondered whether the phasic recruitment of PV neurons is related to a specific movement or reflects a more abstract behavioural variable (Supplementary Fig. 9c). Specifically, the ACC has been implicated in foraging decisions[9,11]—whether to stay or to leave. Therefore, we trained mice on a task version in which they were rewarded at a water port after a fixed 1 s delay from entry. In this task variant, the motor program required for the leaving action was a backward movement (Fig. 4a, cartoon), distinct from the forward movement corresponding to the reward zone exit in the original task version. In addition, this enabled more precise measurements of behavioural timing. Mice stayed inside the port for varying durations (2.0 ± 2.2 s) to consume water reward then exited to initiate the next trial. We found that PV neurons responded with a large phasic firing rate elevation around the time of exit from the reward port (Fig. 4d, Supplementary Fig. 8a, b; 11/12 neurons with activation index > 0, $P < 0.05$, permutation test). Because mice could freely exit at any time, we wondered if the activity of these neurons was modulated by the duration of their stay inside the reward port. Indeed, we observed that the firing rate of PV neurons parametrically increased with longer staying times on a trial-by-trial basis (Fig. 4a–d). A similar representation of stay duration has been found in monkey ACC during a foraging task, which was shown to signal the negative value of staying or equivalently the likelihood of leaving during foraging decisions[9]. This suggests that the graded phasic response of PV neurons in ACC is related to a foraging decision, to leave the reward consumption area and initiate a new run.

Our findings demonstrate that two major classes of interneurons not only provide distinct modes of inhibition but also display unique behavioural correlates, with temporal and functional specificity comparable to principal neurons. Out of the many behavioural events in the task, the homogeneous responses of PV and NS-SOM interneurons bracketed a defined epoch: from reward approach to leaving, and represented a specific behavioural variable, staying time at the reward zone, critical for foraging decisions, a central function attributed to ACC[9,10]. How can this temporal and behavioural specificity be

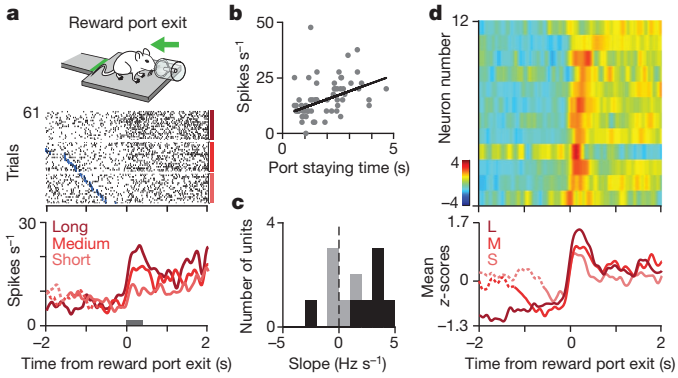

Figure 4 | PV interneurons in the ACC signal stay duration at foraging decisions. **a**, Mouse exiting the reward port (inset). Response of a PV neuron during reward port exit. Raster is sorted by staying time in the port and grouped into terciles. Blue ticks denote water valve offset. PETH is shown for each tercile. **b**, Linear regression between firing rate of the neuron in **a**, (epoch indicated by a grey bar) and staying time is significantly positive ($r = 0.16$, slope, 3.63, $P < 0.005$). **c**, Histogram of regression slopes for all PV neurons. Black bars indicate significant ($P < 0.05$) regression. **d**, Top, z-scored PETHs of 12 PV neurons aligned to reward port exit sorted according to latency of half-peak firing. Bottom, average PETH for PV population grouped into staying time terciles. L, M and S denote long-, medium- and short-staying times, respectively.

understood in the context of our current knowledge of interneurons? First, tuning specificity may arise from the dense, convergent local input these interneuron types receive[7,29], enabling them to 'summarize' local neural activity, which may be particularly high at the moments when a region is engaged in a task[30]. Second, PV interneurons have been implicated in controlling pyramidal cell output[12,14,16], consistent with the synchronous firing and strong inhibitory coupling we observed. In contrast, SOM neurons are thought to gate long-range inputs to principal cells[13,15,17,20], and their asynchronous activation and weaker inhibitory impact on firing output is consistent with this role. In our behaviour, input and output regulation might be expected around the foraging decision, consistent with the observed suppression of NS-SOM interneurons during approach followed by the activation of PV interneurons at reward exit. Taken together, our findings suggest a conceptual model in which these interneuron subtypes specialize in temporally regulating the flow of information in a given cortical circuit during the behavioural events relevant to that area. In summary, these observations bolster the long-held hope that probing identified cell-types will reveal the intrinsic logic of cortical circuits under more natural behavioural settings[5,6].

METHODS SUMMARY

All procedures involving animals were carried out in accordance with National Institutes of Health standards as approved by the Cold Spring Harbor Laboratory Institutional Animal Care and Use Committee.

Full Methods and any associated references are available in the online version of the paper.

Received 27 August 2012; accepted 10 April 2013.
Published online 26 May 2013.

1. Constantinidis, C., Williams, G. V. & Goldman-Rakic, P. S. A role for inhibition in shaping the temporal flow of information in prefrontal cortex. *Nature Neurosci.* **5,** 175–180 (2002).
2. Machens, C. K., Romo, R. & Brody, C. D. Functional, but not anatomical, separation of "what" and "when" in prefrontal cortex. *J. Neurosci.* **30,** 350–360 (2010).
3. Narayanan, N. S. & Laubach, M. Top-down control of motor cortex ensembles by dorsomedial prefrontal cortex. *Neuron* **52,** 921–931 (2006).
4. Wallis, J. D. & Kennerley, S. W. Heterogeneous reward signals in prefrontal cortex. *Curr. Opin. Neurobiol.* **20,** 191–198 (2010).
5. Isaacson, J. S. & Scanziani, M. How inhibition shapes cortical activity. *Neuron* **72,** 231–243 (2011).
6. Klausberger, T. *et al.* Brain-state- and cell-type-specific firing of hippocampal interneurons *in vivo*. *Nature* **421,** 844–848 (2003).
7. Markram, H. *et al.* Interneurons of the neocortical inhibitory system. *Nature Rev. Neurosci.* **5,** 793–807 (2004).
8. Hartwich, K., Pollak, T. & Klausberger, T. Distinct firing patterns of identified basket and dendrite-targeting interneurons in the prefrontal cortex during hippocampal theta and local spindle oscillations. *J. Neurosci.* **29,** 9563–9574 (2009).
9. Hayden, B. Y., Pearson, J. M. & Platt, M. L. Neuronal basis of sequential foraging decisions in a patchy environment. *Nature Neurosci.* **14,** 933–939 (2011).
10. Kolling, N., Behrens, T. E., Mars, R. B. & Rushworth, M. F. Neural mechanisms of foraging. *Science* **336,** 95–98 (2012).
11. Quilodran, R., Rothe, M. & Procyk, E. Behavioral shifts and action valuation in the anterior cingulate cortex. *Neuron* **57,** 314–325 (2008).
12. Atallah, B. V., Bruns, W., Carandini, M. & Scanziani, M. Parvalbumin-expressing interneurons linearly transform cortical responses to visual stimuli. *Neuron* **73,** 159–170 (2012).
13. Gentet, L. J. *et al.* Unique functional properties of somatostatin-expressing GABAergic neurons in mouse barrel cortex. *Nature Neurosci.* **15,** 607–612 (2012).
14. Lovett-Barron, M. *et al.* Regulation of neuronal input transformations by tunable dendritic inhibition. *Nature Neurosci.* **15,** 423–430 (2012).
15. Murayama, M. *et al.* Dendritic encoding of sensory stimuli controlled by deep cortical interneurons. *Nature* **457,** 1137–1141 (2009).
16. Royer, S. *et al.* Control of timing, rate and bursts of hippocampal place cells by dendritic and somatic inhibition. *Nature Neurosci.* **15,** 769–775 (2012).
17. Kapfer, C., Glickfeld, L. L., Atallah, B. V. & Scanziani, M. Supralinear increase of recurrent inhibition during sparse activity in the somatosensory cortex. *Nature Neurosci.* **10,** 743–753 (2007).
18. Ma, Y., Hu, H., Berrebi, A. S., Mathers, P. H. & Agmon, A. Distinct subtypes of somatostatin-containing neocortical interneurons revealed in transgenic mice. *J. Neurosci.* **26,** 5069–5082 (2006).
19. McGarry, L. M. *et al.* Quantitative classification of somatostatin-positive neocortical interneurons identifies three interneuron subtypes. *Front. Neural Circuits* **4,** 12 (2010).
20. Silberberg, G. & Markram, H. Disynaptic inhibition between neocortical pyramidal cells mediated by Martinotti cells. *Neuron* **53,** 735–746 (2007).
21. Hippenmeyer, S. *et al.* A developmental switch in the response of DRG neurons to ETS transcription factor signaling. *PLoS Biol.* **3,** e159 (2005).
22. Taniguchi, H. *et al.* A resource of Cre driver lines for genetic targeting of GABAergic neurons in cerebral cortex. *Neuron* **71,** 995–1013 (2011).
23. Sohal, V. S., Zhang, F., Yizhar, O. & Deisseroth, K. Parvalbumin neurons and gamma rhythms enhance cortical circuit performance. *Nature* **459,** 698–702 (2009).
24. Lima, S. Q., Hromádka, T., Znamenskiy, P. & Zador, A. M. PINP: a new method of tagging neuronal populations for identification during *in vivo* electrophysiological recording. *PLoS ONE* **4,** e6099 (2009).
25. Csicsvari, J., Hirase, H., Czurkó, A., Mamiya, A. & Buzsáki, G. Fast network oscillations in the hippocampal CA1 region of the behaving rat. *J. Neurosci.* **19,** RC20 (1999).
26. Cardin, J. A. *et al.* Driving fast-spiking cells induces gamma rhythm and controls sensory responses. *Nature* **459,** 663–667 (2009).
27. Fujisawa, S., Amarasingham, A., Harrison, M. T. & Buzsáki, G. Behavior-dependent short-term assembly dynamics in the medial prefrontal cortex. *Nature Neurosci.* **11,** 823–833 (2008).
28. Xu, X. & Callaway, E. M. Laminar specificity of functional input to distinct types of inhibitory cortical neurons. *J. Neurosci.* **29,** 70–85 (2009).
29. Ascoli, G. A. *et al.* Petilla terminology: nomenclature of features of GABAergic interneurons of the cerebral cortex. *Nature Rev. Neurosci.* **9,** 557–568 (2008).
30. Isomura, Y., Harukuni, R., Takekawa, T., Aizawa, H. & Fukai, T. Microcircuitry coordination of cortical motor information in self-initiation of voluntary movements. *Nature Neurosci.* **12,** 1586–1593 (2009).

Supplementary Information is available in the online version of the paper.

Acknowledgements This work was supported by grants from the Klingenstein, John Merck, Sloan and Whitehall Foundations to A.K. and the National Institute of Neurological Disorders and Stroke (National Institutes of Health) grant R01NS075531. B.H. received support from the Swartz Foundation and Marie Curie International Outgoing Fellowship within the EU Seventh Framework Programme for Research and Technological Development (2007-2013). D.K. received support from The Robert Lee and Clara Guthrie Patterson Trust Postdoctoral Fellowship and Human Frontier Science Program (2008–2011). We are grateful to K. Deisseroth, E. Boyden, A. Reid and A. Zador for constructs, B. Burbach and R. Eifert for technical assistance, and to J. Lisman, B. Mensh, S. Shea and A. Zador for comments and discussions.

Author Contributions D.K., S.R. and A.K designed experiments. D.K. and S.R. set up and performed experiments. B.H. developed the optical tagging index. D.K., S.R., B.H. and A.K. analysed data and wrote the paper. H.T. and J.Z.H. generated SOM-Cre mice, discussed results and edited the paper.

Author Information Reprints and permissions information is available at www.nature.com/reprints. The authors declare no competing financial interests. Readers are welcome to comment on the online version of the paper. Correspondence and requests for materials should be addressed to A.K. (kepecs@cshl.edu).

METHODS

Microdrive construction. We designed two microdrive models that enabled concurrent optical stimulation and recording of neuronal activity. The plastic frame for the drives was designed using AutoCAD Inventor (Autodesk) and 3D printed (Vista Technologies). In one microdrive model (3.5 g) the frame can house up to 10 individually moveable shuttles and is well suited to record and optically activate large population of neurons. Each shuttle has precision holes drilled to attach the tetrode and/or optical ferrule and a miniature screw (0.6 mm outer diameter, 12 mm length) with a pitch of 160 μm. An electronic interface board (EIB32, Neuralynx) connects tetrodes to the preamplifier (HS36, Neuralynx). The fibre-optic probe for optical stimulation consists of a polyimide coated multimode fibre (60 μm diameter, Polymicro Technologies) glued into a fibre-optic ferrule (LC ferrule 80 μm, Precision Fibre Products). The ferrule end is polished using standard optical methods for efficient light coupling and the other end is precisely cleaved for insertion into the brain. The other microdrive model can house up to 5 independently adjustable shuttles and weighs 2.2 g when loaded with a single shuttle driving a bundle of 6 tetrodes and an optical fibre (Supplementary Fig. 1e).

Viral injection. Adeno-associated virus (AAV) 2/9 serotype (8×10^{12} genome copies per ml, UNC Vector Core Facility) carrying EF1a-DIO-ChR2-EYFP or EF1a-DIO-Arch-EYFP construct[23] was injected into 1-month-old PV-Cre and SOM-Cre male mice. Mice were anaesthetized with an intraperitoneal injection of ketamine-xylazine mixture (0.1 mg per gram body weight ketamine, 0.01 mg per gram body weight xylazine). Exposed skin surfaces were occasionally irrigated with lidocaine. A small craniotomy was made above the left dorsomedial prefrontal cortex (2 mm anteroposterior, 0.5 mm mediolateral, from bregma). Virus was injected with a glass micropipette using a Picospritzer (General Valve). Pulses (20–60) of 10 ms duration were delivered at 0.2 Hz starting from a depth of 1.9 mm from the brain surface up to 1.2 mm in 100 μm steps, waiting a minimum of 2–3 min per site to allow diffusion of the virus. Animals were allowed to recover for at least 2 weeks for optimal viral expression.

Microdrive implantation. After anaesthesia a ~1-mm diameter hole was drilled through the skull at the site of viral injection. Animals received supplementary dose of anaesthetic at 30–90-min intervals to maintain depth of anaesthesia. The microdrive was positioned with the help of a stereotaxic arm (David Kopf Instruments) above the craniotomy with protruding tetrodes. The optical fibre and tetrodes were gradually lowered to a depth of 500 μm from the brain surface. Two 0.25-mm diameter stainless steel wires (Alpha Wire Company) were stripped at the end and inserted into cerebellum and right parietal lobe to a depth of ~1 mm below dura to serve as reference and ground electrodes respectively. Two miniature watch screws (Micro-Mark) were fixed into the parietal plates as anchors. The microdrive was secured to the skull with ultraviolet light curable dental cement (Vitrebond Plus) followed by a layer of black dental acrylic (Lang Dental). Tetrodes and optical fibre were lowered by a further 320 μm before mice recovered from anaesthesia. For post-operative analgesia, ketoprofen (2 mg per kilogram body weight) was administered intraperitoneally. Mice were allowed to recover for at least a week.

Foraging task, behavioural setup, training. The behavioural setup consists of an elevated linear track (length 45 cm, width 5 cm) that connects two 8×10 cm platforms (termed 'reward zone' and 'trigger zone'). Water rewards were delivered at the reward zone either through a lick tube at the end of the reward zone (Fig. 3a) or a water port designed to precisely monitor timing of port entry and exit (Fig. 4a, inset). Position of the mice on the track was monitored at 30 Hz with a spatial resolution of 2 mm pixel^{-1} using a video tracker that tracked one red and one green light-emitting diode (LED) integrated into the preamplifier on the microdrive (Neuralynx). The behavioural hardware (valves, light-sensors) and the laser were triggered through a data acquisition board (National Instruments PCI-MIO-16E-1) controlled by custom MATLAB programs (MathWorks). Position was tracked by Cheetah recording software (Neuralynx). Owing to the additional weight of the preamplifier and cable we used a custom-designed commutator and counterbalance assembly to enable mice to run more freely. The counterbalance consists of a 40-cm boom moving freely on air bearings with a spherical socket at the end acting as an air-bearing commutator. Precisely controlled and frictionless counterbalancing force was achieved using a pneumatic actuator. The tether was suspended by a hollow ball glued to it that floated inside the socket, and was connected to a slip-ring commutator (PSR-27, Neuralynx) to release torque accumulated by the tether.

One to three weeks after surgery, mice were trained to run on the track. In the initial phase of training, mice were provided with water whenever they approached either the reward zone or poked into the water port. After consuming 20–40 rewards, mice were conditioned to obtain water by running to the opposite end of the platform, the trigger zone, and running back to collect the reward. Entry into the trigger zone activated an auditory cue, which signalled availability of water at the reward zone. Once mice performed about 60 runs we introduced different reward sizes (small: 2–4 μl, large: 6–12 μl) signalled by distinct auditory cues (mixture of high frequency and low frequency tones, 0.1 s duration). Mice also received a reminder auditory cue immediately after exiting the trigger zone (Fig. 3a). On a small fraction of trials (15%) reward was omitted. Mice performed 60–200 trials per session lasting 1–2 h. Animals were kept on a water restriction schedule to maintain 85–90% of free-drinking weight.

Recording and and optical stimulation of genetically identified interneurons. Electrophysiological recordings were performed using a Neuralynx Cheetah 32 system. Electrical signals were split and separately amplified and filtered for local field potentials (LFPs) and single unit activity. The signal was band-pass filtered between 600–6,000 Hz and sampled at 32 kHz to record spiking activity, while LFPs were filtered between 0.1–400 Hz and acquired at 3 kHz. We used 6 tetrodes and one optical fibre to record a total of 1,339 single units from 12 mice. Of these, 1,034 neurons (from 4 PV-Cre and 6 SOM-Cre mice) were recorded during the foraging task and 305 neurons (from 2 PV-Cre mice) were recorded in the port variant of the same task. We recorded a total of 28 PV cells from ACC in 5 PV-Cre animals (5, 5, 6, 2 and 10 cells from each animal out of 15, 14, 19, 24 and 41 sessions, respectively) and 35 cells from 6 SOM-Cre animals (14, 4, 2, 3, 10 and 2 cells per animal with 29, 12, 16, 17, 13 and 12 sessions, respectively). In addition we recorded one PV-Cre animal that gave no tagged neurons. Neurons that had baseline firing rate <1 Hz or showed no activity during perievent periods (window size was specific for each event, see below) were excluded from behavioural analyses.

An optical multimode fibre (55 μm diameter NA = 0.7, Polymicro Technologies) was coupled via a modified LC–LC type connector to a multimode fibre (126 μm diameter, numerical aperture = 0.27, CablesPlus USA), which collected light from a blue laser (473 nm; 20 mW; CrystaLaser). Maximal power at the tip of the fibre ranged from 10% to 30% of power at the light source resulting in 2–6 mW of total output at the fibre tip.

To evaluate the spatial extent of light on brain tissue we conducted (1) photobleaching experiments to measure the area with bleached fluorophore and (2) c-Fos staining around the fibre tip. For photobleaching experiments, blue light (473 nm, 2–4 mW power) was applied continuously for 1 h, whereas for c-Fos induced expression we applied the same light for 1 h in 1 ms pulses at 20 Hz. The spread of light in photobleaching experiments was ~1,000 μm (dorso-ventral axis) by 500 μm (medio-lateral axis). Maximum c-Fos induction occurred within a 0.5 mm^2 area (Supplementary Fig. 4a–c). Because our tetrodes were well within 500 μm from the tip of the optical fibre, light reach is not expected to be a limiting factor for optical tagging.

To avoid a photo-electric artefact due to light stimulation[32], we positioned our tetrodes parallel to the fibre and in cases where we saw an artefact, we minimized it by lowering the light intensity. We verified the validity of optical tagging by comparing the average peak-aligned spontaneous waveform with average light evoked waveform using Pearson's correlation coefficient ($r > 0.85$).

The light stimulation protocol (15–30 min) for optogenetic tagging was performed at the end of each recording session consisting of 1–2 ms light pulses at 4, 10, 16, 40 and 100 Hz frequencies. The fibre and tetrodes were lowered 20–40 μm every day after each recording session. At the end of the experiments, electrolytic lesions were made through individual leads of each tetrode on which a tagged neuron was recorded. We only included optically tagged neurons that were mapped to the anterior cingulate cortex based on the cytoarchitectonic structure of the prefrontal cortex[33].

To reveal the morphology of SOM interneurons we used MADM[34] to visualize the arborisation of these interneurons at single cell resolution.

Data analysis. All data analysis was carried out using built-in and custom-built software in MATLAB (MathWorks).

Spike sorting. Spikes were manually sorted into clusters (presumptive neurons) off-line based on peak amplitude and waveform energy using MClust software (A.D. Redish). Cluster quality was quantified using isolation distance[35] and L-ratio[36]. Clusters with isolation distance <18 or L-ratio >0.2 were excluded (median isolation distance, 29; median L-ratio, 0.033, see Supplementary Fig. 2a, b). Autocorrelation functions were inspected for all putative cells. In cases in which the autocorrelation showed absolute refractory period violations, we improved cluster separation, otherwise, the cluster was excluded.

SALT. We developed a statistical test to determine whether optogenetic activation caused a significant change in the timing of spikes after stimulation onset (Supplementary Fig. 11). The distribution of first spike latencies relative to the light pulse, assessed in a 10 ms window after light-stimulation, was compared to epochs of the same duration in the stimulus-free baseline period. The choice of a 10 ms window size provided sufficient statistical power without limiting the number of detected neurons. To measure the distance between these distributions, we used an information theoretic measure (modified Jensen–Shannon divergence)[37]. Using this metric, we tested the hypothesis that the post-stimulus spike-latency distribution is different from a set of baseline distributions for low frequency

light stimulation (4 or 10 Hz) yielding a *P*-value for significant short-latency light-activation. (See Supplementary Notes for a detailed description and http://kepec-slab.cshl.edu/software/ for MATLAB implementation). Note that we also employed a spike shape correlation measure to ensure that our spike sorting was not compromised due to high laser intensities[38]. This is a complementary test as it pertains to spike sorting, whereas SALT tests light effects assuming that spike sorting is correct.

Detection of light-induced inhibition. To detect light-induced inhibition we first determined the putative suppression period using an adaptive smoothing procedure and then evaluated the statistical significance of the firing rate suppression compared to a stimulus-free baseline. First, spike rasters were convolved with a variable kernel Gaussian function to provide a spike density function (SDF) estimate. The kernel width of the Gaussian window was adapted to the local estimate of spiking probability to implement stronger smoothing when information was sparse. Variance was mapped onto spiking probability between 0 (moving average, corresponding to probability of 0) and infinity (Dirac-delta, corresponding to probability of 1). Next, minimal firing was assessed as the minimum of the SDF within 100 ms from light pulse onset. The baseline firing rate was calculated from mean firing probability within a 100 ms window before the start of a pulse train. If the minimal firing after stimulation was lower than 50% of baseline firing rate, then we determined the putative suppression period as the epoch between the half-baseline crossings before and after the minimum. The statistical significance of this suppression was determined by comparing the spike count distribution within this suppression period with an equivalent baseline period using the Mann–Whitney *U*-test ($P < 0.05$). Note that we used a 50% baseline minimum to provide sufficient statistical power to the spike rate comparison and to avoid false detection of random fluctuations in firing rate.

Cross-correlation analysis. Cross-correlations between spike trains were calculated using 1-ms bin size and their statistical significance was evaluated using a modified temporal shuffling method. To infer putative monosynaptic interactions from extracellularly recorded neurons it is critical to rule out co-firing arising from slow time-scale covariations, for instance due to common input[39,40] or oscillatory modulations[41]. Under the assumption that spike trains are independent of one another, the shift predictor can be used to establish the expected level of firing co-occurrence. However, common input or other slow-time scale fluctuations can create trial-to-trial co-variations independent of synaptic interactions. We dealt with the issue of multiple time-scale effects in two ways. First, we used spectral filtering to remove slow time-scale interactions for which shuffle techniques are ill-suited. Second, we next used temporal shuffling to determine the expected level of correlations.

First, the full-length cross-correlation function was computed and high-pass filtered at 4 Hz. For the shuffling, we pseudo-randomly selected 5,000 instances of 30 ms windows from the filtered cross-correlation function, between 100 ms and 5 s time lags. This is equivalent to calculating the cross-correlation of time-shifted data (sometimes called the shuffling method[25,42,43]). The cross-correlation function was then low-pass filtered at 4 Hz to calculate the slow trends previously filtered out (see above). This slow modulation was added back to the shuffled cross-correlations to obtain estimates of cross-correlation that are not distorted by the filtering procedure. This step is necessary to make the shuffled and the original cross-correlations comparable. Significance limits (set to 0.001 for these analyses) were computed based on the distribution of the shuffled cross-correlations. Statistically significant short-latency suppression after a presynaptic spike is generally taken as evidence for monosynaptic inhibitory connections[27,44] and our results examining identified inhibitory neurons bolster this inference.

For group averages, cross-correlations were standardized by subtracting the mean and dividing by the standard deviation of the shuffled cross-correlograms. Pairwise cross-correlation was performed only on units recorded from different tetrodes to avoid artefactual dips (0 ± 750 µs) in cross-correlogram due to the censored period (spike detection dead time), imposed by spike triggering. For PV and SOM 'CC-partners' (wide spiking neurons with significant inhibitory cross-correlations with PV and SOM interneurons) we also included units from the same tetrodes. Inhibition onto CC partners was considered significant only when dips in cross-correlogram were significant beyond +1 ms for two or more bins. We included spikes collected during behavioural sessions and excluded spikes occurring during the optical tagging epochs.

Identification of putative PV interneurons for cross-correlation analysis. We identified putative PV neurons (pPV) based on three criteria: response profile similarity to identified PV neurons, high firing rate (>15 Hz) and narrow spike width (<270 µs). The combination of these three features enabled us to identify a distinct cluster of pPV neurons. Note that our selection algorithm differs from previous studies in that we could make use of the homogeneous firing pattern of identified PV expressing interneurons with respect to behavioural events (Supplementary Fig. 12a). We only selected putative PV interneurons from the second experiment (Fig. 4) incorporating the water port for precise measurement of exit time, that showed the most homogeneity, thus enabling us to confidently isolate putative PV cells. Also note that our aim was not to find all PV neurons, which appeared as false negatives in our data set due to insufficient ChR2 expression or limited light power, but rather to find some cells that resemble identified PV cells enough to conclude with high confidence that they belong to the PV group. We identified 11 putative PV interneurons. Of these neurons, 3 pairs were recorded simultaneously and 2 were recorded along with identified PV cells, yielding 5 new pairs altogether. We found that 4 out of 5 pairs showed significant short latency interaction in cross-correlograms (3 pairs showed both inhibition and synchrony, 1 pair showed synchrony only) (Supplementary Fig. 12b).

Response modulation index and Gap statistics. In order to quantify and compare the selectivity of neural responses to behavioural events, PETHs ($\pm$ 0.5-s window, 50 ms resolution) were calculated for all neurons with reference to each event (reward zone exit, reward zone entry, trigger zone exit, trigger zone entry, water valve on). Significance limits were assessed by upper and lower 0.005 percentiles of shuffled PETHs. Shuffling was performed with a similar method to cross-correlation analysis, with random shifts between the firing rates and the events ranging from 10 to 30 s, shuffling was performed 2,000 times). Response modulation index for each neuron and event was computed as the standard deviation of the PETH. To compute overall selectivity profiles, modulation indices for significantly modulated PETHs was averaged for different neuronal populations (PV, SOM and not tagged) for each event (Supplementary Fig. 6f).

Hierarchical clustering was performed on response profiles with respect to three behaviourally relevant events (reward zone entry, reward zone exit and cue presentation) using squared Euclidean distance measure, averaged over the three events. Number of clusters was iterated ranging from 1 to 100 and the gap statistic[45] was calculated to assess the number of clusters naturally present in the data set (see full description of this in Supplementary Notes).

Activation and suppression indices. The modulation indices (activation index for reward zone exit and suppression index for the reward zone entry events) were both calculated using receiver operating characteristic (ROC) analysis to provide a graded measure and a significance value associated with them[46]. These indices represent scaled version of ROC area (AUC) between two firing rate distributions before and after the event (window size, 0.4 s). We scaled the AUC so that it ranges from -1 to 1 with the sign denoting whether a neuron is activated or suppressed.

Modulation index $= 2\ (\mathrm{ROC}_{\mathrm{area}} - 0.5)$ and $\mathrm{ROC}_{\mathrm{area}} = \int_{-\infty}^{\infty} P(f_{\mathrm{before}} = f) P(f_{\mathrm{after}} < f) df$ in which f_{before} and f_{after} refer to the firing rates before and after the relevant event. Statistical significance was evaluated using a permutation test, in which trial order was pseudo-randomly shuffled 1,000 times to yield a *P* value.

Preference index. To compute preference index during various behavioural epochs, trials were divided into two groups according to cue (cue 1 and cue 2), staying time (shorter and longer than median staying time) and reward size (small and large reward). Firing rates within a fixed peri-event time window (200 ms for cue, 1 s for staying time, and 500 ms for reward preference) were compared using ROC analysis identical to activation and suppression indices. A significant cue preference index of less than 0 means that the neuron preferentially fires for cue 1, whereas more than 0 means preference for cue 2, similarly for staying time preference (long $= -1$, short $= 1$), and reward preference (small $= -1$, large $= 1$).

Staying time modulation of firing rates. We assessed the dependence of firing rate at the reward port on staying time after exit from the reward port on a trial-by-trial basis using robust regression. To determine activation for PV neurons, a window of 0–0.4 s was used.

Bootstrap test of homogeneity and firing rate modulation. We performed the following bootstrap tests to compare PV PETHs aligned to reward zone exit to the not tagged population.

For the test of homogeneity, the within-group homogeneity of the PV population was computed by averaging pair-wise correlations (Pearson correlation coefficient) of *z*-scored PETHs aligned to the reward zone-exit event. This estimate of homogeneity was then tested against the average pair-wise correlation calculated for randomly selected groups of not tagged neurons with the same sample size (1,000 bootstrap samples).

For the test of firing rate modulation, the phasic positive modulation of PV neurons was quantified by the average correlation between PV PETHs aligned to reward zone exit and a template of event-locked firing rate increase. This template was computed as mean *z*-scored PETH of all positively modulated not tagged neurons ($P < 0.05$, activation index > 0, $n = 107$, permutation test). This estimate of positive firing rate modulation for PV neurons was tested against a bootstrap sample of similar estimates for not tagged neurons in the same manner as for the 'test of homogeneity' (see above).

31. Chow, B. Y. *et al.* High-performance genetically targetable optical neural silencing by light-driven proton pumps. *Nature* **463,** 98–102 (2010).
32. Han, X. *et al.* Millisecond-timescale optical control of neural dynamics in the nonhuman primate brain. *Neuron* **62,** 191–198 (2009).

33. Van De Werd, H. J. J. M., Rajkowska, G., Evers, P. & Uylings, H. B. Cytoarchitectonic and chemoarchitectonic characterization of the prefrontal cortical areas in the mouse. *Brain Struct. Funct.* **214,** 339–353 (2010).
34. Zong, H., Espinosa, J. S., Su, H. H., Muzumdar, M. D. & Luo, L. Mosaic analysis with double markers in mice. *Cell* **121,** 479–492 (2005).
35. Harris, K. D., Hirase, H., Leinekugel, X., Henze, D. A. & Buzsaki, G. Temporal interaction between single spikes and complex spike bursts in hippocampal pyramidal cells. *Neuron* **32,** 141–149 (2001).
36. Schmitzer-Torbert, N., Jackson, J., Henze, D., Harris, K. & Redish, A. D. Quantitative measures of cluster quality for use in extracellular recordings. *Neuroscience* **131,** 1–11 (2005).
37. Endres, D. M. & Schindelin, J. E. A new metric for probability distributions. *Information Theory. IEEE Trans. Inform. Theory* **49,** 1858–1860 (2003).
38. Cohen, J. Y., Haesler, S., Vong, L., Lowell, B. B. & Uchida, N. Neuron-type-specific signals for reward and punishment in the ventral tegmental area. *Nature* **482,** 85–88 (2012).
39. Brody, C. D. Correlations without synchrony. *Neural Comput.* **11,** 1537–1551 (1999).
40. Averbeck, B. B., Latham, P. E. & Pouget, A. Neural correlations, population coding and computation. *Nature Rev. Neurosci.* **7,** 358–366 (2006).
41. Nikolić, D., Mureşan, R. C., Feng, W. & Singer, W. Scaled correlation analysis: a better way to compute a cross-correlogram. *Eur. J. Neurosci.* **35,** 742–762 (2012).
42. Marshall, L. *et al.* Hippocampal pyramidal cell-interneuron spike transmission is frequency dependent and responsible for place modulation of interneuron discharge. *J. Neurosci.* **22,** RC197 (2002).
43. Hangya, B., Li, Y., Muller, R. U. & Czurko, A. Complementary spatial firing in place cell-interneuron pairs. *J. Physiol. (Lond.)* **588,** 4165–4175 (2010).
44. Barthó, P. *et al.* Characterization of neocortical principal cells and interneurons by network interactions and extracellular features. *J. Neurophysiol.* **92,** 600–608 (2004).
45. Tibshirani, R., Walther, G. & Hastie, T. Estimating the number of clusters in a data set via the gap statistic. *J. R. Stat. Soc. B* **63,** 411–423 (2001).
46. Kepecs, A., Uchida, N., Zariwala, H. & Mainen, Z. Neural correlates, computation and behavioural impact of decision confidence. *Nature* **455,** 227–231 (2008).